*Elinvo (Electronics, Informatics, and Vocational Education)*
Vol 9, No. 2, 2024, pp. 265-273
ISSN 2580-6424 (printed) | ISSN 2477-2399 (online)

# Multi-Objective Optimization of MEMS-based Box Pattern Microheaters Using Response Surface Method

**Onny Setyawati[1*], Moch. Agus Choiron[1], Axel Bangert[2], Carl Sandhagen[2]**

[1]Brawijaya University, Malang, Indonesia
[2]University of Kassel, Kassel, Germany

**Article Info**

***Article history:***
Received August 19, 2024
Revised September 24, 2024
Accepted October 11, 2024

***Keywords:***
Multi-objective; central composite design; box pattern microheater; response surface method

**Abstract**

We present a response surface method to evaluate multi-objective optimization for MEMS-based microheater design. Box pattern, the standard microheater shape, was selected in this study since it has a uniform temperature distribution compared to other patterns. The optimum parameters are used to obtain the maximum total current density and Joule heat. Based on a hybrid of the Response Surface Method and Central Composited Design, the model simulation emerged with 25 sets of Design Experiments. As expected, the voltage is proportional to the increased output temperature and Joule heat of the microheater. Material thermal conductivity, anchor length and thickness of the heating element are included as design variables for the optimization. The microheater thicknesses of 4.23 - 4.55 µm, length of 40 µm and thermal conductivity of materials of approximately between 52 to 66 $Wm^{-1}K^{-1}$ became the optimized results at 1 V input voltage to obtain a maximum Joule heat of $4.9x10^5$ $W/mm^3$ and total current density of $5.6x10^7$ $mA/mm^2$.



***Corresponding Author:***
Email: osetyawati@ub.ac.id

## INTRODUCTION

With the increasing market demand for Micro Electromechanical Systems (MEMS) devices, research in the MEMS field continues to grow. The increase in microfabrication systems enables a much wider range of applications in sensor development. MEMS-based gas sensors are one of the most widely developed sensors for microfabrication applications [1], [2], [3]. In 2018 microheater array powder sintering (MAPS) became a novel additive process in microsystem since it had low power requirements but typically high temperature [4], [5]. The applied microfabrication allows gas sensors to be used in several environments, such as biosensor development, environmental monitoring [6], indoor air quality measurement, nanowires [7] [8], and others [9], [10], [11]. On the internal part of a MEMS gas sensor, there are generally two devices, i.e. a microheater and a temperature sensor. The microheater is used to operate the MEMS gas sensor at high temperatures [12], [13], [14] because the gas sensor requires heat energy to react to the gas, while the temperature sensor functions to measure the working temperature and control the gas sensor. Li et al. used circular and S-shaped or meander heaters designed as flexible devices to be thermally analyzed [15]. Waghmare described nichrome-based microheaters design using COMSOL Multiphysics [16], showing that the temperature distribution of the heating element was increased as the trace width of the serpentine shape as well as the input voltage were increased.

Given the potential utilization of microheaters according to specific requirements, optimizing their usage stands to benefit in terms of saving fabrication costs and time. Following this study, we present a multi-objective model simulation of a box pattern microheater to determine optimum values of total current density and Joule heat. In the model simulation, response surface analysis is employed

by providing either variations in voltage, resistive materials, or the heater dimensions to obtain optimal results. The response surface method (RSM) can identify the optimal working conditions to achieve the maximum or minimum responses, and it helps to understand relationships between input and response variables to improve efficiency and reduce costs. In addition, we simulated the different shapes and several materials of microheaters, to find their localized heating areas and energy efficiency. We focused on box-shaped microheaters not only due to their temperature distribution is more concentrated or localized compared to that of annular or conventional serpentine shapes, but also because they are less complex in design. Review of microheaters along with the applications, design and their fabrication technologies were reported in [17]. Materials, design and fab technology were some factors that could influence the performance of microheaters. The design of parallel heaters by Tiwari [18] presented a resistive heating element on a glass substrate modelled for a serpentine pattern using FEM. The best choice for the microfluidic Polymerase Chain Reaction (PCR) chip used a parallel NiCr resistive element pattern to obtain the best power efficiency and better temperature control [18]. ConventorWare was used for modelling the MEMS resonator in the gas sensor [19] to present temperature distribution for the serpentine shape microheater and temperature sensor, which were increased as the given voltage increased [19]. Four meander designs of microheaters, modelled by varied thicknesses and resistive element materials, suitable for infrared (IR) emitters were then fabricated and exposed in [20].

Model simulation design of the structures using multi objective RSM would help to optimize these microstructures and in turn reduce errors in devices fabrication. RSM can explain multiple parameters of process, i.e. responses, which are simultaneously influenced by multiple input variables through statistical and math equations [15]. The goal of RSM is to reach optimum operating conditions and minimize the experimental attempts [15], [21]. The design procedure for RSM involves the steps of [21]: (a) Designing a series of experiments i.e Design of Experiments (DoE) for certain responses or process parameters. (b) Development of a mathematical model with high order response surface and maximum fitting. (c) Determination of the significant and non-significant experimental parameters for response or sensitivity. (d) Illustration of the direct and interactive effects of parameters. Box Behnken (BB) or Central Composite Design (CCD) as the optimization tools in response surface analysis would study the objective functions to find relationships between design variables [22], [23]. Since BB provided less experimental design points compared to CCD, some simulation models preferred to apply it in the analysis [24], [25], even though it dealt only with three levels of design variables. On the other hand, CCD had a higher number of degrees of freedom. However, BB would be preferable for the manufacturing interests. In this study, we tested both BB and CCD, wherein the DoE sets showed the same number; after that, we used a hybrid of RSM and CCD to evaluate the multi-objective optimization process. This paper is organized as follows. The introduction, as the first part, introduced the research background and previous relevant issues. The model simulation was explained in the methodology part, followed by the results and discussion where the DoE explained, and some factors influenced in the microheater design and characteristics were examined. The conclusion part summarized this study and gave information for future work.

## METHODS

The simulations were carried out using ANSYS Workbench 2021-R1 with thermal-electric analysis system. The microheater had an input voltage and the expected output would be the result of the working temperature, Joule heat and current density produced by the microheater. The standard design of the heating element of microheater was used, viz. the box pattern with trace width of 5 μm. The three-dimensional model simulation was carried out by providing input voltage on one of the beams of the microheater. The evaluation of multi objective optimization was performed using a hybrid of RSM and CCD. Few numbers of trials could be obtained using fit design points offered by RSM. Meanwhile, high efficiency in obtaining global optimum points would be achieved by CCD. The

variables of voltage, anchor length, thickness and thermal conductivity, illustrated in Table 1, were used to achieve maximum Joule heat output and total current density. In the design, the parametric sweep was utilized to vary those parameters. The following equations showed the relationships between those variables with the objective functions.

Table 1. Design parameters of box pattern microheater

| Design parameters | Symbol | Values |
|---|---|---|
| Thickness | P1 | 4 - 8 µm |
| Length of anchor | P2 | 40 - 80 µm |
| Thermal conductivity | P5 | 11.3 - 88 $Wm^{-1}K^{-1}$ |
| Voltage | P6 | 100 - 1000 mV |

$$\text{Joule heat} = f(\text{voltage, thermal conductivity, length, thickness}) \quad (1)$$

$$\text{Total current density} = f(\text{voltage, thermal conductivity, length, thickness}) \quad (2)$$

The design parameters of input voltage of 100 - 500 mV, length of anchor of 40 - 80 µm and element thickness of 4 - 8 µm were initiated. Material thermal conductivities ranging from 11.3 up to 88 $Wm^{-1}K^{-1}$, normally belonging to metal (element and alloy), were given. This property enables efficient heat conduction within microheaters or dissipation into their surroundings to be determined. Figure 1 shows the flowchart for the optimization steps. At first, we initiated the design parameters and the objective functions. BB and CCD were tested in this simulation, and both showed 25 sets of DoE, solving the design of parameters to optimize the maximum outputs of total current density and Joule heat. The DoE setting is given in Table 2, where 25 trials emerged. The configuration of the optimization process gave us 4000 generated samples, wherein 800 samples were used for each iteration.

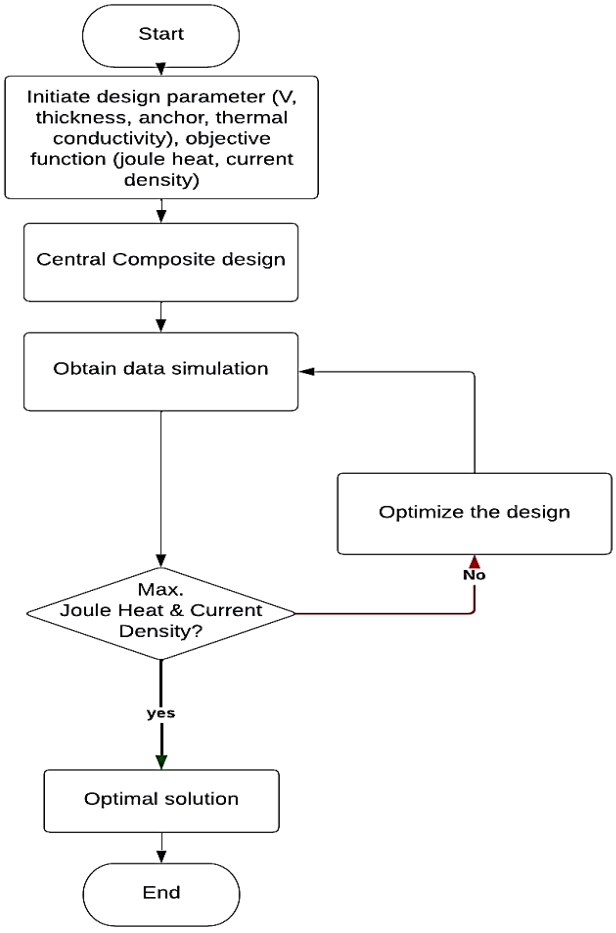


Figure 1. Flowchart of the multi-objective optimization

ISSN 2580-6424 (printed) | ISSN 2477-2399 (online)

Table 2 presents the design parameters of a box-pattern microheater, including key variables such as thickness, anchor length, thermal conductivity, and voltage. Each parameter is defined with its corresponding symbol and value range, which are critical for understanding the structural and functional aspects of the microheater's performance.

Table 2. Design of Experiments of 25 sets

| No. | P1 - Thickness (um) | P2 - length (um) | P5 - Thermal Conductivity ($Wm^{-1}K^{-1}$) | P6 - Voltage Magnitude (mV) | P3 - Joule Heat Maximum ($x10^5$ $Wmm^{-3}$) | P4 - Total Current Density Maximum ($x10^7 mAmm^{-2}$) |
|---|---|---|---|---|---|---|
| 1 | 4 | 45 | 49.650 | 550 | 1.435 | 2.928 |
| 2 | 2 | 45 | 49.650 | 550 | 1.435 | 2.928 |
| 3 | 6 | 45 | 49.650 | 550 | 1.435 | 2.928 |
| 4 | 4 | 40 | 49.650 | 550 | 1.726 | 3.213 |
| 5 | 4 | 50 | 49.650 | 550 | 1.210 | 2.688 |
| 6 | 4 | 45 | 11.300 | 550 | 1.435 | 2.928 |
| 7 | 4 | 45 | 88.000 | 550 | 1.435 | 2.928 |
| 8 | 4 | 45 | 49.650 | 100 | 0.047 | 0.532 |
| 9 | 4 | 45 | 49.650 | 1000 | 4.745 | 5.323 |
| 10 | 2 | 40 | 11.300 | 100 | 0.057 | 0.584 |
| 11 | 6 | 40 | 11.300 | 100 | 0.057 | 0.584 |
| 12 | 2 | 50 | 11.300 | 100 | 0.040 | 0.489 |
| 13 | 6 | 50 | 11.300 | 100 | 0.040 | 0.489 |
| 14 | 2 | 40 | 88.000 | 100 | 0.057 | 0.584 |
| 15 | 6 | 40 | 88.000 | 100 | 0.057 | 0.584 |
| 16 | 2 | 50 | 88.000 | 100 | 0.040 | 0.489 |
| 17 | 6 | 50 | 88.000 | 100 | 0.040 | 0.489 |
| 18 | 2 | 40 | 11.300 | 1000 | 5.707 | 5.842 |
| 19 | 6 | 40 | 11.300 | 1000 | 5.707 | 5.842 |
| 20 | 2 | 50 | 11.300 | 1000 | 4.001 | 4.888 |
| 21 | 6 | 50 | 11.300 | 1000 | 4.001 | 4.888 |
| 22 | 2 | 40 | 88.000 | 1000 | 5.707 | 5.842 |
| 23 | 6 | 40 | 88.000 | 1000 | 5.707 | 5.842 |
| 24 | 2 | 50 | 88.000 | 1000 | 4.001 | 4.888 |
| 25 | 6 | 50 | 88.000 | 1000 | 4.001 | 4.888 |

## RESULT AND DISCUSSION

### *Selecting The Pattern*

Figure 2 shows the temperature distribution for three different shapes at 0.1 V input voltage with a maximum value of 141.5 $^oC$. In the plot, the maximum heating occurred in the center of the comb on the box (Figure 2a) and annular (Figure 2b) microheater. Based on the simulation results, we found that an increase in the input voltage caused an exponential increase in the maximum working temperature of the microheater. Increasing the input voltage results in a higher operating temperature generated by the microheater. However, as the input voltage of 0.1 V up to 2 V was given, there's no significant temperature difference among those four patterns, only 0.01 – 1.78 $^oC$. The box pattern showed the best temperature distribution at the core of the element, indicating potential benefits in minimizing heat dissipation to surrounding areas.

Figures 3 and 4 also show that among four different shapes, i.e. annular, box, modified serpentine, and conventional (typical shape) serpentine, the box pattern microheater exhibited the highest output of total current density and Joule heat. Hence, based on these results, we selected the box pattern to be

optimized using RSM, as it also demonstrated a uniform temperature distribution compared to the other patterns.

We examined and compared the results produced by microheater materials whose range of thermal conductivities is from 11.3 to 88 $Wm^{-1}K^{-1}$. Given its low thermal conductivity, minimizing heat transfer from the resistive element to the substrate would be advantageous, thereby leading to lower power consumption and higher temperatures.

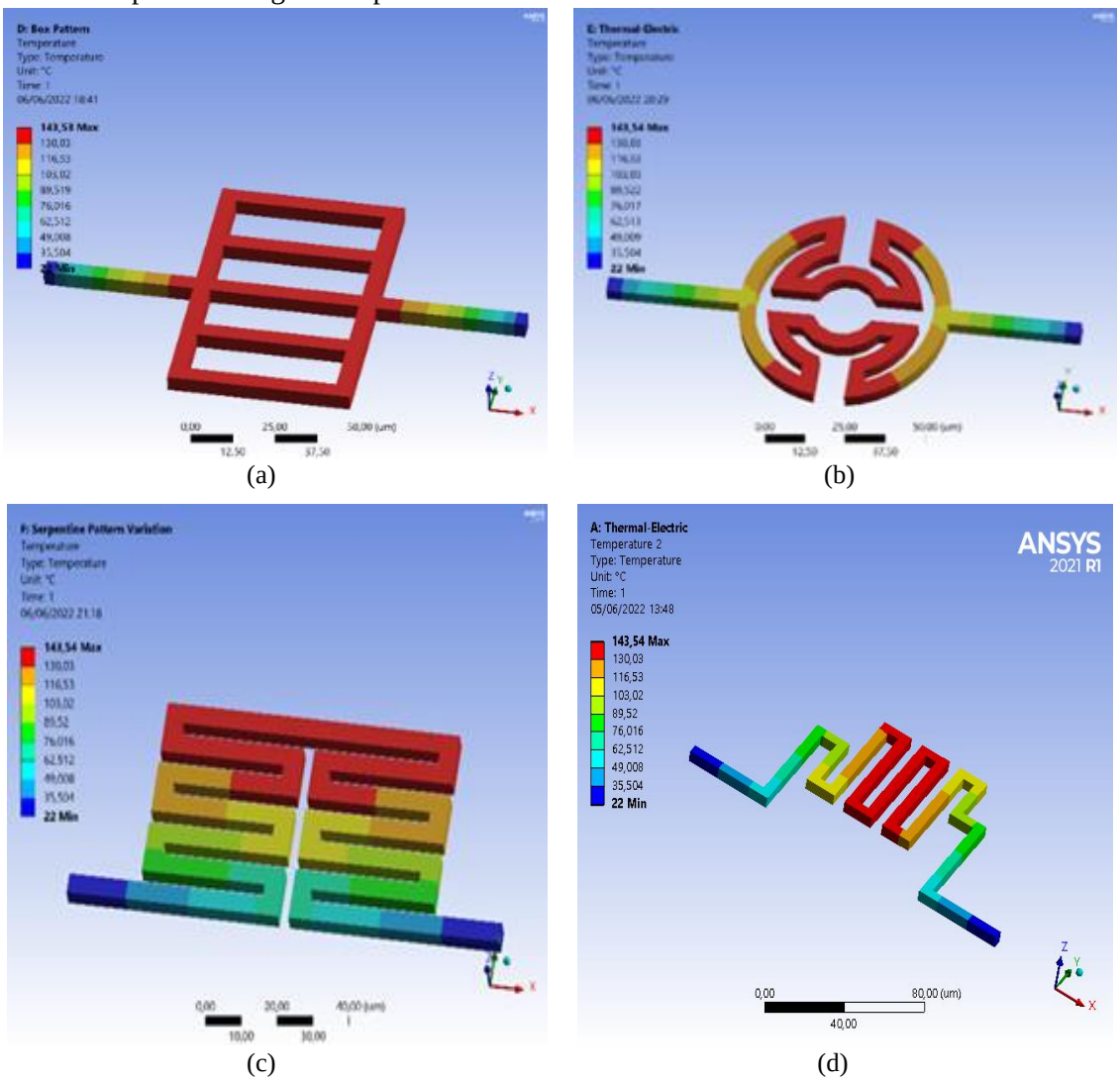


Figure 2. Temperature distribution of (a) The box pattern, (b) The annular pattern, (c) The serpentine (variation shape), and (d) The Typical serpentine pattern at a given input of 0.1 V

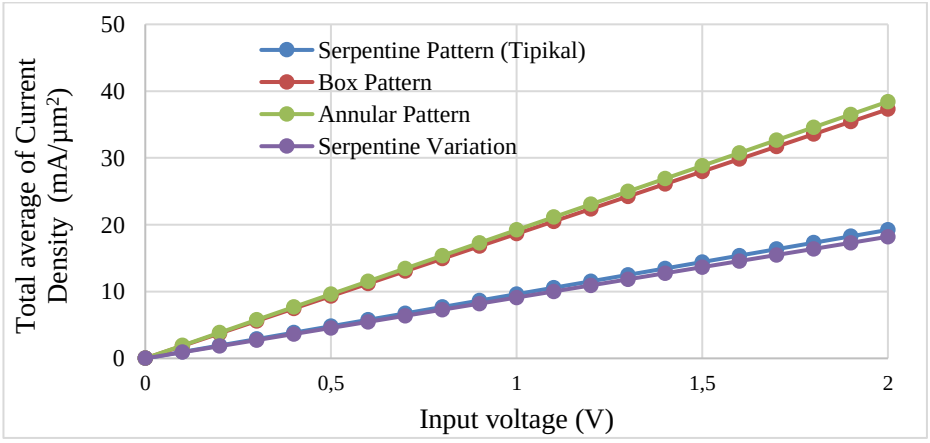


Figure 3. Total current density of the microheaters with varying patterns as a function of input voltage

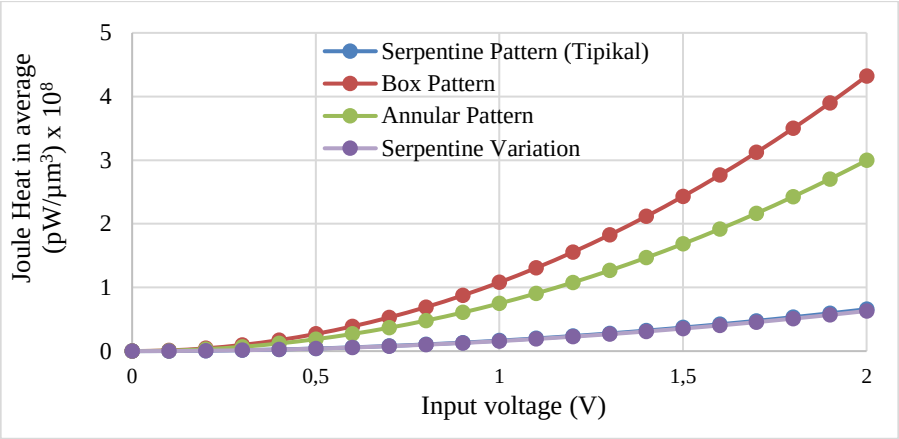


Figure 4. Joule heat of the microheaters with varying patterns as a function of input voltage

***Multi-objective with a Hybrid of RSM and CCD***

Three selected candidates resulted from CCD after a maximum of 20 iterations with 800 samples per iteration, which were summarized in Table 3, showing maximum values of Joule heat of $4.9x10^5$ W/mm$^3$ and total current density of $5.6x10^7$ mA/mm$^2$. The NSGA-II (Non-dominated Sorted Genetic Algorithm-II) has a MOGA (Multi-Objective Genetic Algorithm) type, which is based on controlled elitism concepts. Elitism is one of the genetic operators besides selection, crossover, and mutation; it maintains good solutions without crossover or mutation. MOGA aims to find the global optimum by handling multiple objectives and constraints. The sensitivity bar told us that the length of the microheater anchor showed an inverse proportion strongly to the maximum values of the Joule heat, and so did the microheater thickness. However, the input voltage had a proportional impact on the Joule heat, followed by thermal conductivity in the second place. For the maximum values of the current density, the thickness of the heating element would increase, followed by the input voltage. However, the length and thermal conductivity were inversely proportional to the total current density.

Table 3. Selected candidate CCD for the optimum designs

| No. | Parameter | Value Candidates | | |
|---|---|---|---|---|
| 1 | Thickness (μm) | 4.228 | 4.550 | 4.351 |
| 2 | Anchor length (μm) | 40.003 | 40.013 | 40.001 |
| 3 | Thermal conductivity ($Wm^{-1}K^{-1}$) | 51.625 | 65.962 | 57.699 |
| 4 | Voltage (mV) | 999.75 | 999.69 | 998.98 |

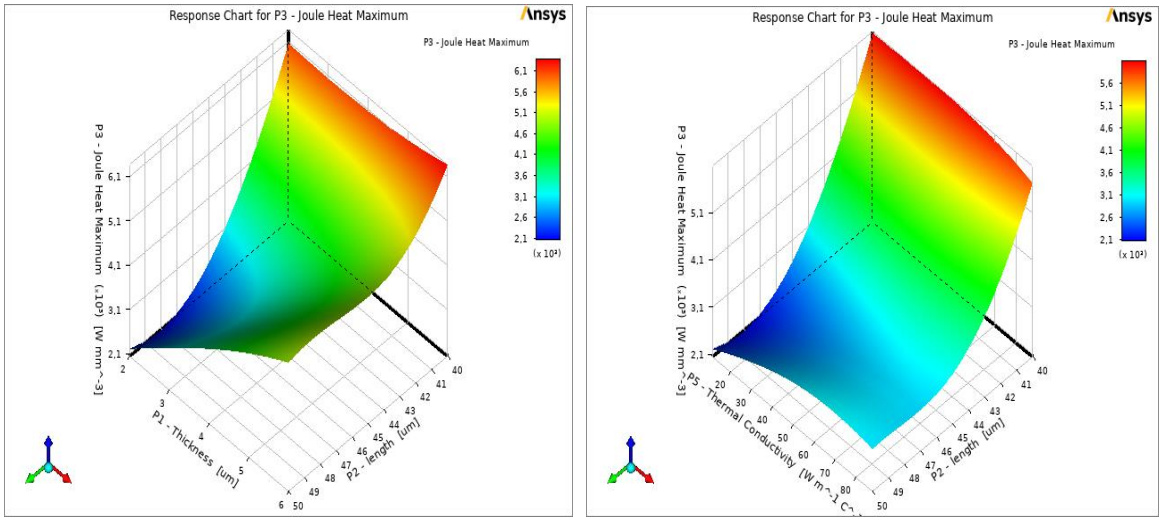


(a) (b)

Figure 5. Maximum values of the Joule heat as a function of three design parameters: (a) Thickness & length, (b) Thermal conductivity & length

Figure 5 shows that a maximum Joule heat of approximately 6x105 W/mm3 could be achieved at the length of 40 µm. However, reducing this length by only 5 µm resulted in a nearly halve in the Joule heat value from its maximum. Regarding the heaters' thicknesses of 2 and 4 µm they yielded $6x10^5$ $W/mm^3$ of Joule heat, and more than 6.35 $x10^5$ $W/mm^3$ at 6 µm. The optimal thickness, however, is around 4 µm (as indicated in the accompanying Table 3) since at the thickness of 6 µm, the total current density reached its minimum value.

Materials with thermal conductivity from 11.3 to 65 $Wm^{-1}K^{-1}$ showed a capability to sustain a high Joule heat output of around $6x10^5$ $W/mm^3$. Meanwhile, materials possessing thermal conductivity in the range of 30 - 80 $Wm^{-1}K^{-1}$ presented current densities ranging from 6.15 $x10^7$ to $6.65x10^7$ $mA/mm^2$. Notably, materials with a thermal conductivity of 88 $Wm^{-1}K^{-1}$ (specifically Aluminum) achieved a current density of $7.05x10^7$ $mA/mm^2$, while the maximum total current density of $7.65x10^7$ $mA/mm^2$ was attained by materials having a thermal conductivity of 11.3 $Wm^{-1}K^{-1}$ (NiCr), as illustrated in Figure 6. Furthermore, optimizing parameters such as an anchor length of 40 µm and a thickness of 2 µm, gave a peak total current density of approximately $7.7x10^7$ $mA/mm^2$. It was observed that increasing both parameters leads to a gradual decrease in total current density.

The optimized conditions for the box pattern microheater design, details in Table 3, indicated that selecting a material with thermal conductivity from 51 to 66 $Wm^{-1}K^{-1}$ was crucial. This selection is feasible for manufacturing purposes, considering that stainless steel, with its thermal conductivity of 62 $Wm^{-1}K^{-1}$, could serve as the resistive element in the microheater. This selection enabled the achievement of a total current density of $6.15x10^7$ $mA/mm^2$ and a Joule heat output of $6x10^5$ $W/mm^3$.

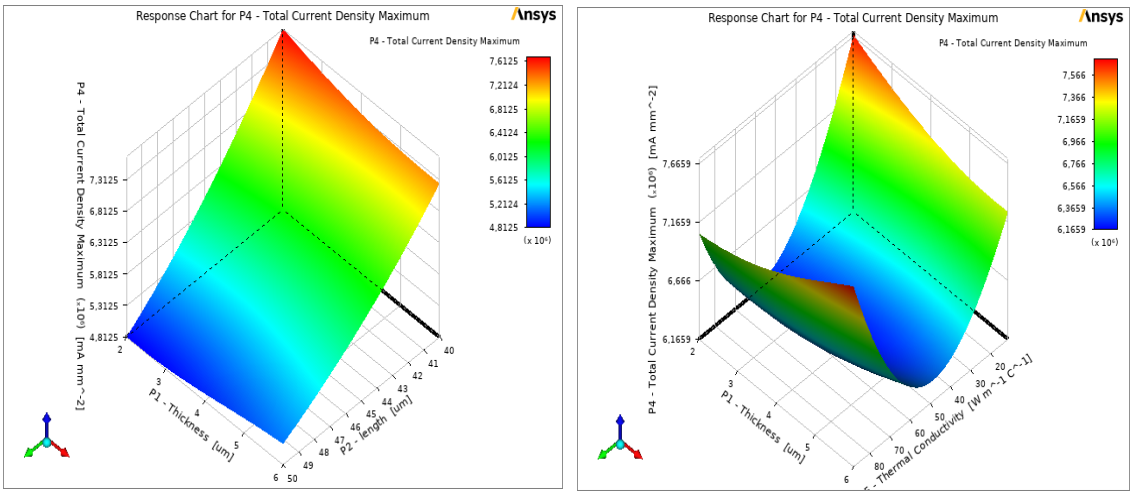


(a) (b)

Figure 6. Maximum values of the total current density as a function of three design parameters (a) Thickness & length, (b) Thermal conductivity & thickness

## CONCLUSION

This paper presents a multi-objective optimization approach for designing a box pattern microheater, with a primary focus on maximizing Joule heat output and total current density. The study utilized a genetic algorithm to propose 25 sets of Design of Experiments (DoE), subsequently narrowing down to three final candidates using Central Composite Design (CCD).

Since the box microheaters are intended for environmental applications, e.g. gas sensors, moisture and temperature monitoring, achieving uniform temperature distribution and maximizing Joule heat and total current density for efficient energy consumption has become the focus of this investigation. The design process involved employing parametric sweep techniques to systematically vary parameters, including anchor length, microheater thickness, thermal conductivity, and input voltage. This systematic approach ensures that the microheater design meets the strict requirements of environmental

applications, where precise control of thermal characteristics is essential for optimal performance and energy efficiency. The most effective way to achieve a high Joule heat output involves reducing the length of the microheater anchor and simultaneously increasing the voltage. However, in achieving a high current density, the thickness of the microheater played an important role. As previously discussed, three optimal candidates emerged after 20 iterations, yielding $4.9 \times 10^5$ W/mm$^3$ of Joule heat output and $5.6 \times 10^7$ mA/mm$^2$ of total current density. All design parameters were optimized thoroughly for an input voltage of 1 V and a length of 40 µm. The thickness parameter was adjusted slightly to align with the thermal conductivity characteristics of the materials used.

For future work, it is essential to identify the appropriate materials to employ, as the current densities are significantly elevated, exceeding the maximum values reported in the literature. Consequently, the findings of this study should be considered a preliminary step, and we must also prioritize the design considerations before integrating the microheaters into other structures.

## ACKNOWLEDGMENT

The authors thank Geraldio R. Safitri (student at Electrical Engineering Dept.) for providing the information on the pattern designs used in this study and the Design and Engineering System Studio at Mechanical Engineering Dept. for technical support.

## REFERENCES

[1] H. Nazemi, A. Joseph, J. Park, and A. Emadi, "Advanced Micro- and Nano-Gas Sensor Technology: A Review," *Sensors*, vol. 19, no. 6, p. 1285, Mar. 2019, doi: 10.3390/s19061285.

[2] J. Cho and G. Shin, "Fabrication of a Flexible, Wireless Micro-Heater on Elastomer for Wearable Gas Sensor Applications," *Polymers (Basel)*, vol. 14, no. 8, p. 1557, Apr. 2022, doi: 10.3390/polym14081557.

[3] Z. Yuan, F. Yang, and F. Meng, "Research Progress on Coating of Sensitive Materials for Micro-Hotplate Gas Sensor," *Micromachines (Basel)*, vol. 13, no. 3, p. 491, Mar. 2022, doi: 10.3390/mi13030491.

[4] N. Holt, L. G. Marques, A. Van Horn, M. Montazeri, and W. Zhou, "Fabrication and control of a microheater array for Microheater Array Powder Sintering," *The International Journal of Advanced Manufacturing Technology*, vol. 95, no. 1–4, pp. 1369–1376, Mar. 2018, doi: 10.1007/s00170-017-1316-8.

[5] N. Holt, A. Van Horn, M. Montazeri, and W. Zhou, "Microheater array powder sintering: A novel additive manufacturing process," *J Manuf Process*, vol. 31, pp. 536–551, Jan. 2018, doi: 10.1016/j.jmapro.2017.12.009.

[6] G. Jung *et al.*, "A low-power embedded poly-Si micro-heater for gas sensor platform based on a FET transducer and its application for NO2 sensing," *Sens Actuators B Chem*, vol. 334, p. 129642, May 2021, doi: 10.1016/j.snb.2021.129642.

[7] S. Sohrabi, L. Hajshahvaladi, M. K. Moraveji, E. Sohrabi, and F. Heidarpoor, "Patterned synthesis of nanowires in microheaters: design and operational aspects," *Microfluid Nanofluidics*, vol. 26, no. 1, p. 3, Jan. 2022, doi: 10.1007/s10404-021-02506-y.

[8] J.-H. Kim, A. Mirzaei, H. W. Kim, and S. S. Kim, "Low-Voltage-Driven Sensors Based on ZnO Nanowires for Room-Temperature Detection of NO $_2$ and CO Gases," *ACS Appl Mater Interfaces*, vol. 11, no. 27, pp. 24172–24183, Jul. 2019, doi: 10.1021/acsami.9b07208.

[9] R. M. Krishna *et al.*, "Polysilicon micro-heaters for resonance tuning in CMOS photonics," *Opt Lett*, vol. 47, no. 5, p. 1097, Mar. 2022, doi: 10.1364/OL.441510.

[10] T. Hyodo, K. Nagae, T. Ueda, T. Sasahara, and Yasuhiro Shimizu, "Sensing Behavior of Adsorption/Combustion-type Gas Microsensors to Various Alcoholic Vapors," *Sensors and Materials*, vol. 35, no. 11, p. 3851, Nov. 2023, doi: 10.18494/SAM4403.

[11] D. G. Jung, J. Lee, J. B. Kwon, B. Maeng, H. K. An, and D. Jung, "Low-Voltage-Driven SnO2-Based H2S Microsensor with Optimized Micro-Heater for Portable Gas Sensor Applications," *Micromachines (Basel)*, vol. 13, no. 10, 2022, doi: 10.3390/mi13101609.

[12] M. Prasad and P. S. Dutta, "Development of micro-hotplate and its reliability for gas sensing applications," *Applied Physics A*, vol. 124, no. 11, p. 788, Nov. 2018, doi: 10.1007/s00339-018-2210-4.

[13] A. Lahlalia, O. Le Neel, R. Shankar, S. Y. Kam, and L. Filipovic, "Electro-Thermal Simulation & Characterization of a Microheater for SMO Gas Sensors," *Journal of Microelectromechanical Systems*, vol. 27, no. 3, pp. 529–537, Jun. 2018, doi: 10.1109/JMEMS.2018.2822942.

[14] B. Tang, Y. Shi, J. Li, J. Tang, and Q. Feng, "Design, Simulation, and Fabrication of Multilayer Al2O3 Ceramic Micro-Hotplates for High Temperature Gas Sensors," *Sensors*, vol. 22, no. 18, p. 6778, Sep. 2022, doi: 10.3390/s22186778.

[15] D. Li, Y. Ruan, C. Chen, W. He, C. Chi, and Q. Lin, "Design and Thermal Analysis of Flexible Microheaters," *Micromachines (Basel)*, vol. 13, no. 7, p. 1037, Jun. 2022, doi: 10.3390/mi13071037.

[16] S. Waghmare, M. A. Hasan, S. Manikandan, and S. Datta, "Computational design and analysis of patterned micro-heaters with various thickness and trace width," *J Phys Conf Ser*, vol. 2054, no. 1, p. 012083, Oct. 2021, doi: 10.1088/1742-6596/2054/1/012083.

[17] Z. E. Jeroish, K. S. Bhuvaneshwari, F. Samsuri, and V. Narayanamurthy, "Microheater: material, design, fabrication, temperature control, and applications—a role in COVID-19," *Biomed Microdevices*, vol. 24, no. 1, p. 3, Mar. 2022, doi: 10.1007/s10544-021-00595-8.

[18] S. K. Tiwari, S. Bhat, K. K. Mahato, and B. B. Manjunath, "Design and Simulation of Parallel Microheater," *Frontiers in Heat and Mass Transfer*, vol. 10, Feb. 2018, doi: 10.5098/hmt.10.9.

[19] L. F. Setiawan, G. Witjaksono, and A. Y. Ahmed, "Modeling and Simulation of Thermally Actuated MEMS Resonators for Gas Sensing Applications," in *2018 IEEE Student Conference on Research and Development (SCOReD)*, IEEE, Nov. 2018, pp. 1–5. doi: 10.1109/SCORED.2018.8710897.

[20] C. Paun, R. Tomescu, D. Cristea, O. Ionescu, and C. Parvulescu, "Design, fabrication and caracterization of a micro-heater for metasurface-based gas sensors," in *2020 International Semiconductor Conference (CAS)*, IEEE, Oct. 2020, pp. 31–34. doi: 10.1109/CAS50358.2020.9267975.

[21] R. Tariq, F. Maqbool, and S. Z. Abbas, "Small-scale production of hydrogen via auto-thermal reforming in an adiabatic packed bed reactor: Parametric study and reactor's optimization through response surface methodology," *Comput Chem Eng*, vol. 145, p. 107192, Feb. 2021, doi: 10.1016/j.compchemeng.2020.107192.

[22] T. Suwanda, R. Soenoko, Y. S. Irawan, and Moch. A. Choiron, "The Optimum Process Parameter of Dissimilar Metal AA6061 – AISI304 Continuous Drive Friction Welding," *Journal of Southwest Jiaotong University*, vol. 55, no. 2, 2020, doi: 10.35741/issn.0258-2724.55.2.52.

[23] J. Bayuo, M. A. Abukari, and K. B. Pelig-Ba, "Optimization using central composite design (CCD) of response surface methodology (RSM) for biosorption of hexavalent chromium from aqueous media," *Appl Water Sci*, vol. 10, no. 6, p. 135, Jun. 2020, doi: 10.1007/s13201-020-01213-3.

[24] Z. Liu *et al.*, "Multi-objective optimization of the performance and emission characteristics for a dual-fuel engine with hydrogen addition," *Fuel*, vol. 332, p. 126231, Jan. 2023, doi: 10.1016/j.fuel.2022.126231.

[25] M. Shanmugam and L. Sirisha Maganti, "Multi-objective optimization of parallel microchannel heat sink with inlet/outlet U, I, Z type manifold configuration by RSM and NSGA-II," *Int J Heat Mass Transf*, vol. 201, p. 123641, Feb. 2023, doi: 10.1016/j.ijheatmasstransfer.2022.123641.